JOURNAL OF MATERIALS SCIENCE **34** (1999) 5707–5720

Simulation of prismatic cracking of cooling basalt lava flows by the drying of sol-gels

D. HULL, B. D. CADDOCK
Department of Materials Science and Engineering, University of Liverpool, Liverpool L69 3BX, UK

The progressive development of primary arrays of straight and curved cracks during the drying of thin films of aqueous silica sol-gel is investigated experimentally by direct observations using light microscopy. Three main test configurations are used to generate a range of drying profiles in the sol-gel: (i) films between a glass plate and a flexible glass cover slip; (ii) films between two glass plates held apart by a rigid spacer, and; (iii) uncovered films on a glass plate. Cracks in the primary arrays grow normal to the iso-concentration water profiles. The arrays of primary cracks observed in basalt lava flows and described by Spry (*J. Geol. Soc. Aust.* **8** (1962) 191) i.e. parallel straight columns, chevrons, rosettes, fans, inverted fans and basins, are reproduced in the pseudo two-dimensional films of sol-gel. The development of both primary and secondary cracking patterns is strongly dependent on the constraints associated with the bonding of the sol-gel to the glass and the subsequent splitting of the gel-glass interfaces.

1. Introduction

The regular prismatic columns formed in basalt lava flows, as in the Giant's Causeway in Northern Ireland and in many other sites around the world, are now explained in terms of the stresses associated with differential shrinkage during cooling. It is supposed that the cracks grow normal to the cooling isotherms. Many models have been proposed for the geometry of the columns. Reviews of these models and analyses of the importance of cooling by conduction through the solidified lava, and cooling by convection through the cracks, on the dimensions and shapes of the columns are given in references [1, 2]. The explanation of secondary cracking of these prismatic columns, particularly the cross-fractures, sometimes referred to as 'ball and socket jointing' [3], remains a mystery although various models have been offered. None of these adequately account for the characteristic features of these cross fractures.

Direct experimental work on the development of cracking patterns during cooling of basalt lava flows is difficult. The crack spacing is of the order of 0.3–1.0 m so that exceptionally large volumes of material are involved. The molten lava is at high temperature and the cooling rates mean that the time scales for the growth of cracks (typically 3–10 m long) is very long. Direct observation of growing cracks is impossible except by imprecise indirect methods. Thus, the description and interpretation of the cracking patterns is based primarily on posthumous observations.

The mechanics of crack growth in lava flows must involve a combination of many variables including the rate of cooling, dependent on the thermal properties of the molten lava and solid basalt, the overall shape of the lava flow, mechanical relaxation associated with creep and viscoelastic deformation and the strain energy release during crack growth in large temperature gradients. Much of this information is inaccessible but the interaction between the key variables can be represented by the schematic in Fig. 1a.

Our primary objective in initiating this work was to explain the intriguing cross-fractures in basalt columns. As a preliminary we have sought a system that simulates the cracking processes in basalt that is more accessible to direct experimental study. A similar approach has been described by Müller [4] who studied shrinkage cracks in starch. This material dries to give an ordered, three-dimensional, columnar array with a similar morphology to basalt columns. The system we have chosen is a drying sol-gel in which crack initiation and growth is determined by shrinkage associated with the evaporation of water which transforms the material from a low viscosity liquid, the sol, to a rigid solid, the dried gel. The gel is a silica network. This system has many characteristics closely analogous to the solidification of lava. The kinetics and mechanics of crack growth are controlled by the evaporation of water. Cracks grow in a field with a strong water concentration profile $C(z, t)$ where z is normal to the drying surface and t is time. This simulates the temperature profile in the lava $T(z, t)$. The isotherms of the lava are replaced by lines or surfaces of constant water content (iso-concentration), as illustrated in Fig. 1b. A major difference, that influences the experimental approach,

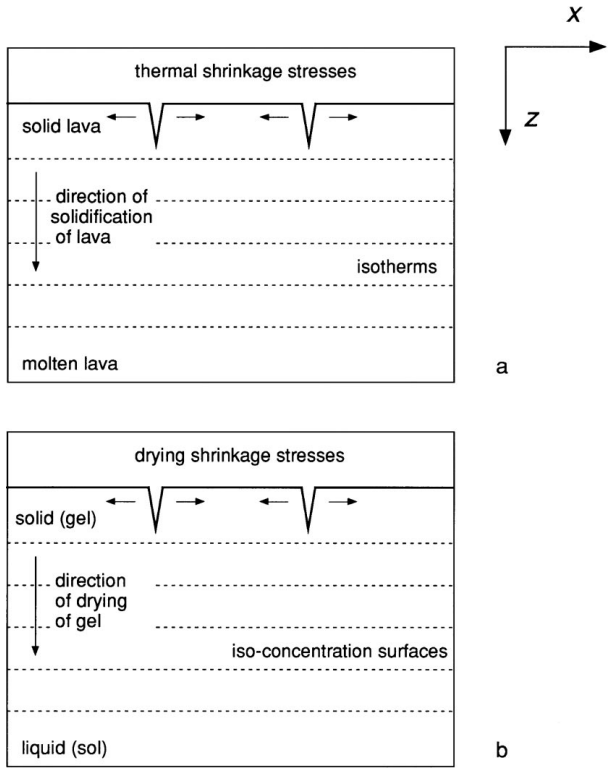

Figure 1 Schematic representation of formation of shrinkage stresses in cooling lava flows and drying sols.

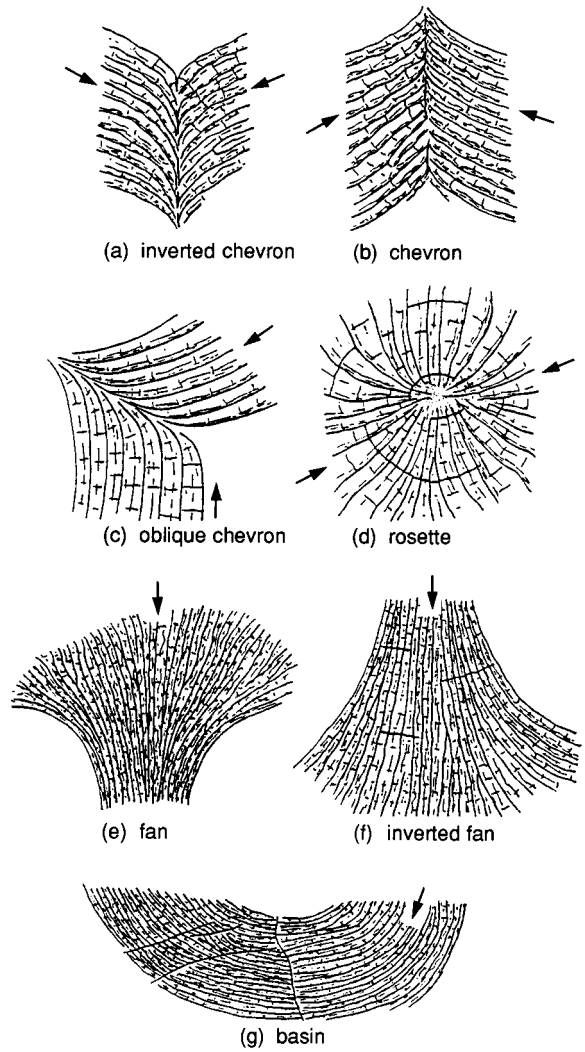

Figure 2 Curved columnar structures formed in basalt lava flows according to Spry [7]. Arrows mark the probable direction of growth of the primary cracks. These were not identified by Spry.

is that there is a large reduction in volume of the gel before it becomes sufficiently rigid for the shrinkage to induce cracking.

The sol-gel used in this study was transparent, in both the liquid and solid states, so allowing direct observation of the deformation and cracking events. The microstructure of the sol-gel had dimensions of less than 0.1 μm. This ensured that cracking phenomena, on the scale of microns, could be investigated in a material that was effectively homogeneous, with no direct influence of the microstructure on the paths of the cracks. Cracking associated with silica sol-gel desiccation is reviewed in Iler [5] and Brinker and Scherer [6].

To make an assessment of the value of the sol-gel system in simulating the cracking patterns of basalt lava we chose to attempt to reproduce directly the main patterns illustrated by Spry [7] in his review of the cracking of basalt. These are reproduced in Fig. 2 and are referred to by Spry as "common structures formed by curved columns." The drawings are two-dimensional representations of three-dimensional arrays of cracks.

The patterns illustrated in Fig. 2 summarise a large number of field observations. They show a primary array of cracks (representing columns) which produce the dominant features of the patterns. This determines the nomenclature: chevron, rosette, fan and basin. Following earlier work [8–10] Spry assumed that the growth of the primary cracks was normal to the isotherms. The patterns also show ill-defined secondary cracks lying approximately normal to the primary cracks. These are referred to as 'cross fractures.' In quiescent stable conditions a planar static lava flow cools uniformly from the top and bottom surfaces with isotherms parallel to these surfaces. This results in an array of straight parallel columns normal to the surfaces. It is supposed that the curved columnar structures form when cooling is non-uniform as in the entablature that forms between two sets of columnar cracks from the top and bottom surface of the flow, and in regions of non-planar flow, as in irregular dykes and sills.

The field observations rarely reveal the direction of growth of the primary cracks. This makes the distinction between the three chevron patterns (Fig. 2a–c) problematic. They are in effect the same pattern providing it is assumed that the primary cracks grow in the direction indicated by the arrows. The two fan patterns (Fig. 2e and f) are also the same but there is a distinction if the primary cracks grow in the directions indicated.

In this paper we describe the experimental simulation of these patterns using a quasi-two-dimensional geometry. Inevitably, three-dimensional effects occur that complicate the interpretation but we attempt to minimise or isolate these.

An important feature of prismatic cracking of lava is the development of large numbers of cracks. This phenomenon is widely observed in many material situations and is usually referred to as 'multiple cracking.' Thus, experimental observations that model multiple

cracking have a direct relevance, outside those of columnar jointing, in areas such as damage development in composite materials, crack patterns in mud, ceramic coatings, brittle films on plastics, glazes on pottery, cracking of oxide films and the flow processes and drying mechanisms of printing inks and paints.

2. Materials and experimental procedures

2.1. Silica sol-gel

A commercial aqueous silica sol was used in all the experiments. The product, identified as Ludox TM-50, is marketed by Du Pont. Ludox TM-50 is a mobile liquid with a silica content of 50 wt %, the remainder being water except for a small amount of alkali to stabilise the sol at a pH of about 9.0. In some experiments Ludox TM-50 was diluted with water to give a lower silica content and reduce the viscosity of the sol. In a sealed container the sol is stable at room temperature for several months. In an open container the water evaporates and the sol transforms to a gel. Loss of water leads to large shrinkage strains that can result in shrinkage cracks; the density of the cracks and the cracking patterns depend on the external and internal constraints during drying.

The sequence of events during the drying of a sol-gel is complex [6]. As the water evaporates from the surface of the sol the silica particles (mean particle size 30 nm [11]), dispersed in water, approach each other. Silanol groups on the surface of the particles interact in a condensation reaction to form oxygen bridges linking the particles into extended three-dimensional chains. As drying proceeds the chains link up to form a continuous network with an open structure. The liquid becomes a viscoelastic gel which increases in stiffness as further evaporation occurs. Eventually, the gel becomes a rigid solid consisting of an aggregate of chains of silica particles with inter-connecting pores. Removal of the last traces of water requires extended heating at elevated temperatures.

The correlation between water content, specific volume and material properties such as shrinkage and viscoelasticity are difficult to determine and have not been measured in this work. In the context of the experiments described in the next section some appreciation of the inter-relation between cracking and drying was obtained by measuring the weight loss of a film of TM-50 sandwiched between two glass slides, see inset in Fig. 3. The bottom glass slide was 1 mm thick and the upper slide was a 0.1 mm thick, 18 mm square, cover slip. A drop of liquid was placed on the bottom slide and this was covered with the cover slip. The liquid formed a square film with the same dimensions as the cover slip. The initial thickness of the liquid film was about 50 μm. The data is shown in Fig. 3. Equivalent data for the drying of an uncovered circular drop of film of TM-50 with a similar weight is also shown.

Evaporation was restricted to the edges of the square film. Weight loss was rapid at the beginning and it started to level off between 30 and 40%. A similar result was obtained for the uncovered circular film. Evaporation of the uncovered film occurs from a surface about 10 times greater in area than for the covered film. However, the rate of evaporation, per unit area of surface, is greatest at the edges of the film where the radius of curvature is smallest. Complete drying of the TM-50, to a weight loss of 50%, was achieved by heating to 200 °C.

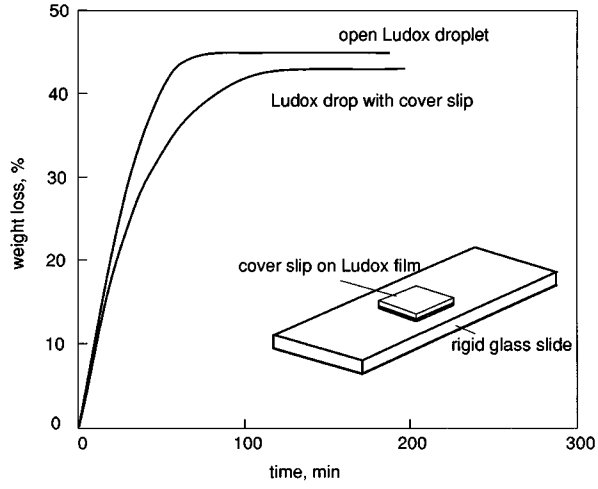

Figure 3 Drying profiles of Ludox TM-50 drops, with and without a cover slip, in air at 20 °C.

Cracking started in the uncovered film after about 13 min and was complete after 40 min, sometime before the drying curve started to level off. The onset of cracking corresponds to an overall weight loss of 15% and cracking is complete after an overall loss of 40%. A similar result was obtained for the covered film, with cracking initiating after 5 min. In all tests cracking initiated at the edges of the covered film and the open drop. This was followed by a complex sequence of cracking processes as the rest of the sol dried, as described in Sections 3 and 4. The cracking patterns influence the diffusion paths for the moisture and the concentration gradients in the drying sol-gel.

2.2. Direct observation of development of crack patterns

A number of test procedures were developed during this work. It has been possible to generate a very wide range of patterns from conventional mud cracks to highly aligned two-dimensional linear arrays of 'columnar' cracks. These patterns are determined by the drying profiles generated in the test samples and the external constraints to shrinkage. The experiment with the cover slip described in the previous sub-section was complicated because, as evaporation proceeded, shrinkage resulted in the formation of shrinkage cavities in the un-gelled liquid in the centre of the disk and the deflection of the thin cover slip drawn in by the surface tension between the liquid and the drying gel and the glass. The drying sequence and the crack patterns depended on the thickness of the cover slip, the amount of sol, and the interface properties between the drying TM-50 and the glass.

All the experiments reported in this paper were made by observing cracking in thin films. Three experimental configurations were used: (i) films between two rigid glass plates; (ii) films between a single rigid plate and a flexible cover slip, and; (iii) uncovered drops and films

on a rigid glass plate. Except in the late stages of drying, the sol and gel remained transparent throughout the drying process. Direct continuous observations of the drying process and the nucleation and growth of cracks were made using transmitted and reflected light microscopy. The optical axis of the microscope was normal to the plane of the glass plates. Variations in thickness of the films and the development of delamination and cracking parallel to the plates was determined from interference patterns in reflected light and through-thickness differential focusing. The cracking and deformation processes were clearly visible in both reflected and transmitted light.

3. Deformation and cracking processes in sol-gels

In this section we describe one example of the sequence of cracking in a film to illustrate the influence of drying profiles and external constraints on the development of cracking patterns and the sequence of cracking. In this way we demonstrate the origin of the main features of the patterns we have produced that simulate the patterns formed in basalt lava (Fig. 2) described in the next section.

The main features of the cracking process are shown in Fig. 4. This is a partially cracked film between a rigid glass slide and a square flexible cover slip. The progressive development of this pattern is shown in more detail in Fig. 5. The initial thickness of the film was about 5 μm. The image in Fig. 4 was obtained in reflected light and shows the formation of a set of primary cracks and the development of delamination or splitting (shown by the bright areas) between the glass and the solidified gel. In this experimental configuration there are two such interfaces; splitting at one interface always precedes splitting at the other. The diffuse boundaries a-b and a′-b′ mark changes associated with the transformation from a liquid sol to a rigid gel. The primary cracks approach the boundary a′-b′ but never cross it. These cracks are normal to a′-b′ and so form normal to the water concentration profiles. Inside the boundary a-b the sol is a mobile liquid. High resolution light microscopy of this region revealed rapid movement of impurity particles as the liquid flowed to the boundary to feed the large amount of shrinkage that occurred before the sol changed to a gel and became rigid.

Initially, all the primary cracks grew normal to the edges of the square cover slip and then developed into curved arrays. Away from the corners the cracks remained normal to the edges and formed a parallel array of cracks equivalent to the regular columns that form in basalt lava. An example of such an array is shown in Fig. 6. The image in Fig. 6a was obtained in transmitted light and the image in Fig. 6b in reflected light. The detail in Fig. 5 shows that cracking occurred progressively. Cracking was complete after about 30 min. Both primary cracking and delamination occurred somewhat erratically. At times the cracks grew smoothly and continuously and at other times in a stop-go mode. Fig. 5a shows an early stage of crack formation; the cracks nucleated at the edges of the film. The liquid-solid boundary corresponding to a-b in Fig. 4 is clearly visible. The feature marked X is a small void in the sol which did not move during cracking. The average spacing of the primary cracks, W, is approximately 15 μm.

In separate experiments the ratio W/p for films between two glass slides was measured and the data is shown in Fig. 7; p is the thickness of the film. For thin films (5–150 μm) a flexible cover slip was used. The thickness was varied by controlling the amount of sol. After cracking the cover slip was removed and the dimensions of individual laths were measured using a light microscope. A wider range of thicknesses was obtained by making a wedge of sol between two rigid glass slides separated at one end by a spacer. The sol was introduced into the wedge cavity. After drying there was a continuous variation of crack spacing

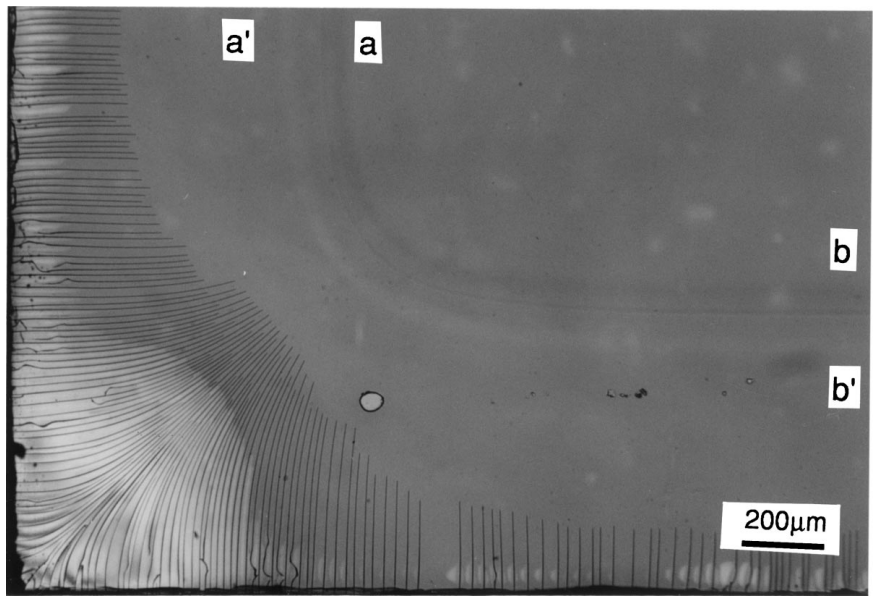

Figure 4 Reflected light microscope image of corner of a square cover slip, on a film of sol-gel supported on a rigid glass slide, showing a partially cracked film. An array of primary cracks has formed at the edges of the cover slip and grown into the film. Subsequently, delamination has occurred at the glass-gel interfaces producing a bright image.

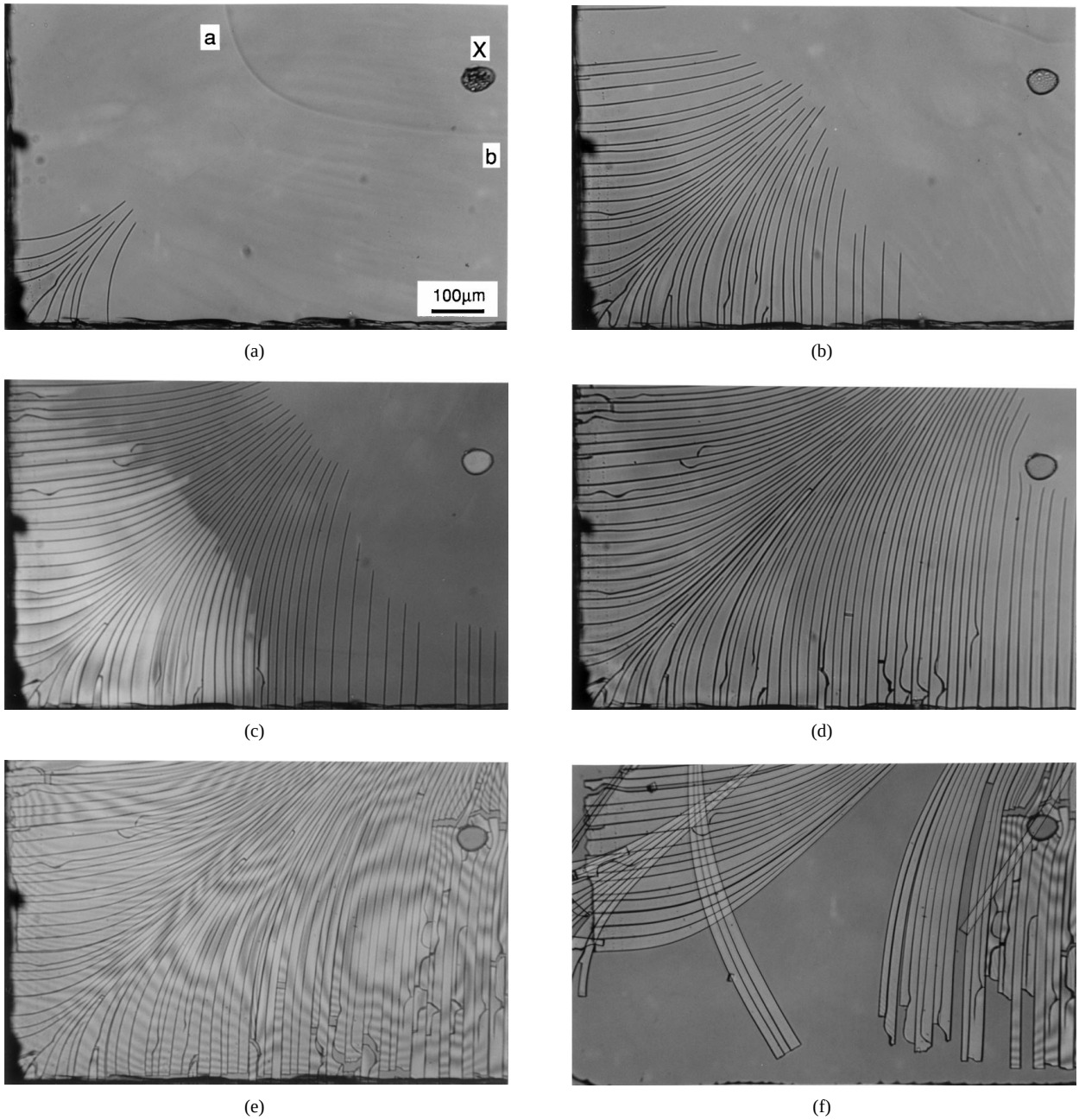

Figure 5 Progressive development of primary cracks and delamination in specimen illustrated in Fig. 4. Figs 5a, b and d taken in reflected light and Figs 5c, e and f taken in transmitted light.

along the length of the wedge. This was measured in a light microscope without separating the glass slides. The thickness of the film along the wedge was determined from the dimensions of the wedge. This approach is similar to the method described by Allain and Limat [12] who also measured W/p using spacers of different thickness to obtain a range of values of p. The data is included in Fig. 7. The broken line in Fig. 7 corresponds to $W/p = 3$. There is reasonably good agreement between the present results and those of Allain and Limat. However, it should be emphasised that no systematic experiments have been made to evaluate the effect of drying variables, such as rate of evaporation and concentration gradients, on W/p. These may account for some of the scatter in Fig. 7.

The individual cracks in the array grow erratically although the average speed of the cracks is the same. In the curved arrays some of the cracks stop, and others are nucleated, depending of the pattern, so that the crack spacing-film thickness ratio remains approximately constant. However, with a flexible cover slip the film thickness varies as drying of the film progresses so that the average spacing changes. Thus, in the example in Fig. 5, the film thickness decreased as the cracks grew so that the average spacing decreased. Figs 5b and c were taken at approximately the same time and illustrate the difference between the images produced in transmitted and reflected light. Some secondary cracking is apparent in Fig. 5d. The appearance of the film after cracking is complete is shown in Fig. 5e. Further secondary cracking has occurred. The complex fringe pattern results from multiple scattering and interference from light scattered from surfaces formed by delamination at both glass-gel interfaces. At this stage the cover slip can be readily removed and thin laths or filaments of solid material lie loosely on the glass surface (Fig. 5f).

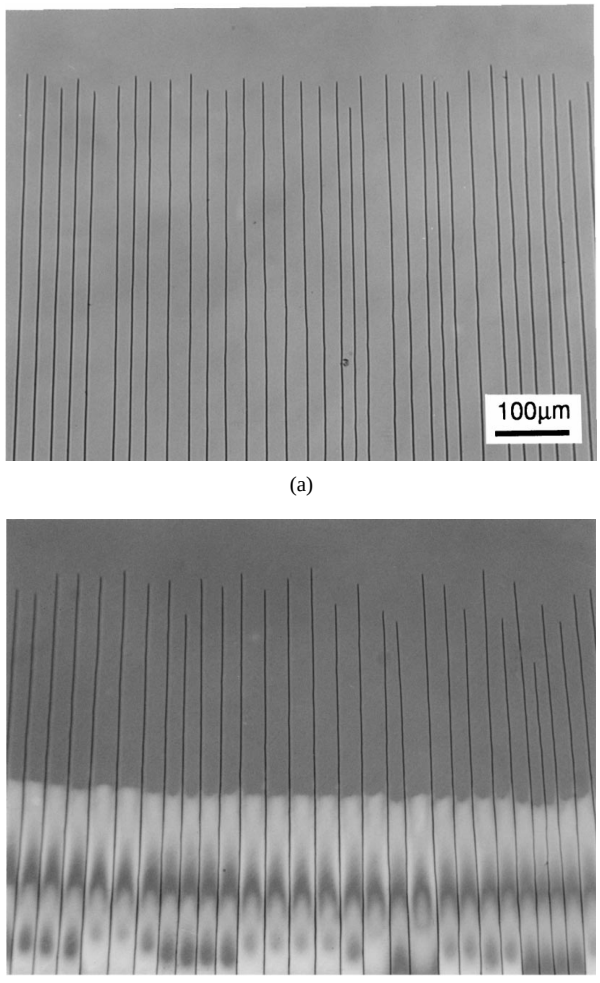

Figure 6 Parallel arrays of cracks viewed in: (a) Transmitted and; (b) reflected light, illustrating the approximately uniform spacing and the erratic progress of the cracking front.

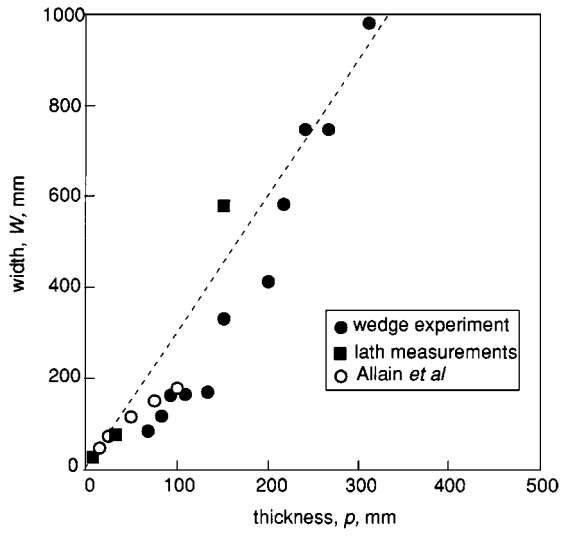

Figure 7 Variation of crack spacing with thickness of film determined by different methods.

The sequence of primary, secondary and delamination cracking in this example is, in part, related to the configuration used. The large reductions in volume that occur before the material is sufficiently rigid to crack are accommodated by liquid flowing from the centre to the edges and the overall thickness of the film decreases. When the outer rim of the film becomes rigid further reductions in the thickness of the film become non-uniform and the cover slip deforms elastically so that the film becomes thinner in the middle. Eventually, a shrinkage cavity forms in the centre of the film.

Further shrinkage of the rigid or semi-rigid gel occurs after the primary array of cracks has formed. This leads to delamination and secondary cracking because the constraints are non-uniform. Since the main emphasis of this paper is the development of the array of primary cracks this aspect is not developed here. However, some features of the cracking process, that are not apparent in the example displayed in Figs 4 and 5, require a brief explanation because they relate to the interpretation of the patterns shown in the next section.

The constraints during drying of a film, without a cover slip, are significantly different from those for a film formed between two glass plates. Shrinkage normal to the film is less constrained so that the onset of delamination is delayed. However, the later stages of shrinkage are non-uniform, through the thickness, so that after the formation of the primary cracks the filaments curl away from the glass plate. In contrast, for a film bounded by two rigid plates held a fixed distance apart during drying the shrinkage normal to the film produces large constraints at a much earlier stage of the drying process. Primary and delamination cracks are closely associated and in some cases the primary cracks grow ahead of the delamination and in others the sequence is reversed. Both sets of growing crack fronts are closer to the liquid boundary. The delamination cracks grow in a stop-go mode and traces of successive positions of the crack front are left in the film and on the glass surface because of plastic relaxation at the tip of the stopped cracks. In this test configuration some cracking also occurs, parallel to the glass-sol interface, through the semi-rigid gel. Most of these features are displayed in the patterns formed in the 'basin' and 'inverted fan' patterns shown in the next section.

A schematic representation of most of the cracking features described in this section is shown in Fig. 8. These are section diagrams normal to the plane of the film and parallel to the direction of growth of the primary cracks. In addition to the cracking processes shear deformation of the semi-rigid gel occurs before the primary cracks form, as illustrated in Fig. 8a. Shear banding was observed for all the test configurations and was readily observed by varying the optical conditions in the microscope. The primary cracks grew through the region of shear deformation. Shear occurred in discrete bands which were at approximately $\pm 45^\circ$ to the primary cracks. An example of primary cracks that have grown through shear bands is shown in Fig. 9.

4. Simulation of curved columns in lava flows

Following the discussion in Section 1 we identify five independent patterns from Spry's diagram in Fig. 2. They are chevron, rosette, fan, inverted fan and basin. In this section we illustrate the formation of each of these patterns in a drying sol-gel. More complicated patterns have been produced but they are essentially combinations of these simple patterns.

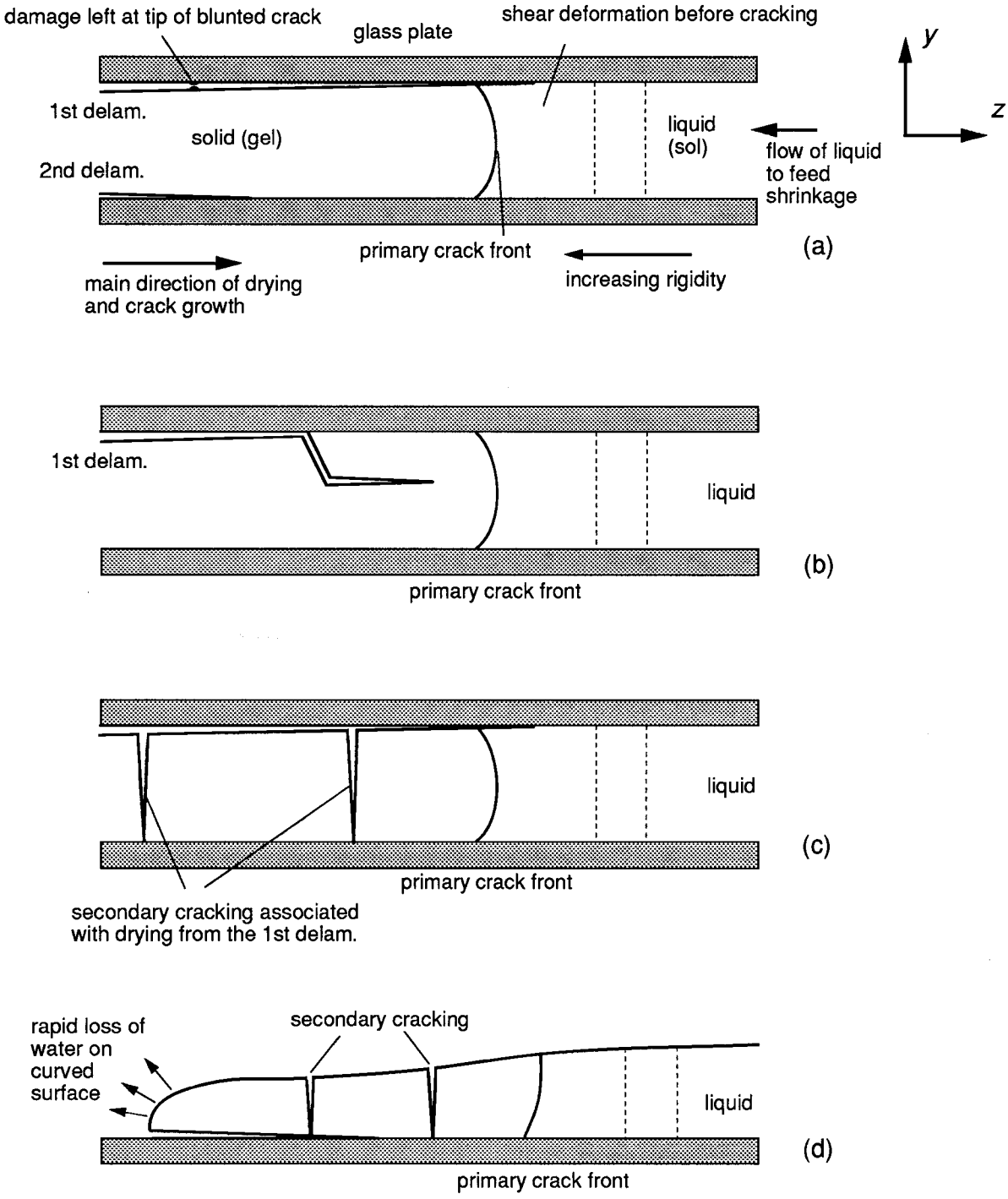

Figure 8 Schematic of cracking processes of drying sol-gel films: (a) Crack formation between two glass plates with a primary crack and delamination cracks; (b) primary crack and a delamination crack developing into a crack through the sol-gel parallel to the glass plates; (c) primary crack and secondary cracks that have grown at the drying surface of a delamination, and; (d) primary crack, secondary cracks and a delamination crack in an uncovered film (note the change in shape of the film as it dries).

The choice of the experimental configurations used to produce the patterns was somewhat arbitrary. We have used the three approaches described in Section 2 and selected examples that illustrate the effects in the most elegant way. In all the examples the direction of growth of the primary cracks is shown by the arrows.

Rosettes. The crack patterns in Fig. 10 formed in films of sol without a cover slip. Fig. 10a is for diluted Ludox with 30% silica on a glass surface. Primary cracking started at the outer edge of the film and the cracks grew radially to the centre. At a later stage delamination cracks formed at the glass-gel interface. As drying progressed the thickness of the film varied (see Fig. 8d) and in the centre of the rosette final shrinkage of the liquid left a very thin film. When the radial cracks reached the centre the internal stresses in the individual laths led to marked bending away from the glass surface. This relaxed the internal stresses in the laths so that no secondary cracks occurred. Similar observations have been reported recently by Allain and co-workers [13–15].

The pattern in Fig. 10b formed in the centre of a larger, approximately square film of undiluted TM-50 (50% silica). This was thicker than the film in Fig. 10a. Primary cracking was followed by delamination. Some of the internal strains in the laths (or columns) were

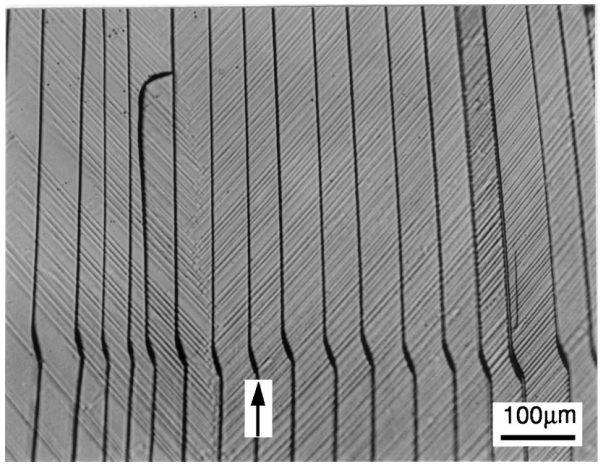

Figure 9 Parallel array of cracks that have grown through shear bands.

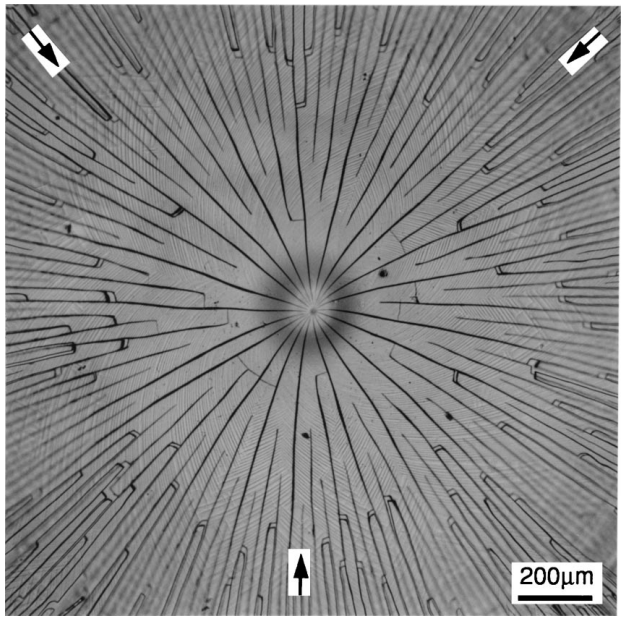

(a)

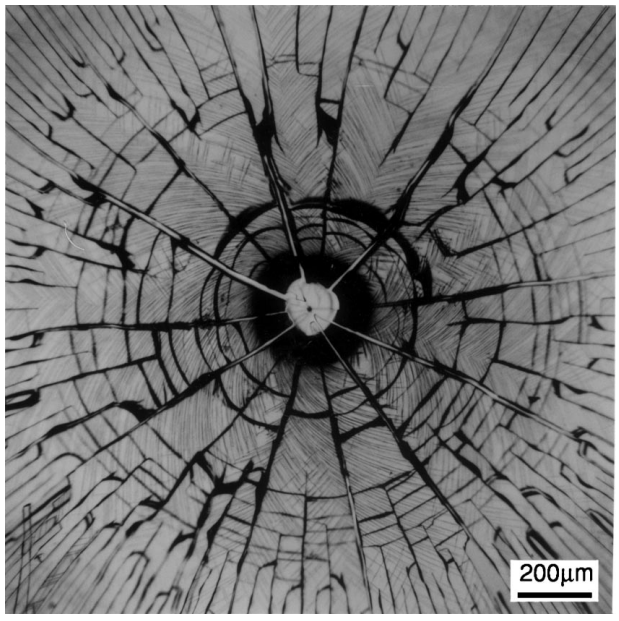

(b)

Figure 10 Rosette patterns of cracks formed in uncovered films: (a) Thin film of diluted TM-50 Ludox with 30% silica; (b) thicker film of undiluted TM-50 Ludox.

relieved, before delamination, by secondary cracking. These cracks developed as non-continuous concentric rings, about the centre of the rosette, approximately normal to the primary cracks. There is a shrinkage cavity in the centre of the rosette.

Chevrons. The technique for producing the chevron patterns shown in Fig. 11 was similar to that used for the rosettes. A drop of TM-50 was placed on a slide and then smeared into a streak approximately 3 mm wide and 20 mm long. Drying and cracking started at the rounded ends of the streak forming semi-rosette patterns at each end as illustrated schematically in Fig. 11a. Later 'columnar' parallel cracking occurred at the edges of the streak where the drying front became parallel to the sides. The chevron pattern, Fig. 11b, formed in the region between the semi-rosettes and the parallel patterns, formed under the influence of drying from the sides and from the ends.

The film was thinner at the edges of the streak and the cracks were more closely spaced, approaching the limit of resolution of the light microscope. The crack spacing increased progressively towards the centre of the streak. Examples of the increase in crack spacing are evident at the sides of the image in Fig. 11b.

In exposed thin films drying occurred in about 5 min. The direction of growth of the cracks, marked on Fig. 11, was readily followed in the microscope. The curvature of the cracks, producing the chevron pattern, results from the drying profiles. If it is assumed that the main direction of primary crack growth is normal to the iso-concentration lines it is possible to map the position of these lines as illustrated in Fig. 12. As the chevron cracks approached each other the crack paths are influenced by the interaction of the local stress fields as well as the more global stress fields arising from shrinkage. The cracks curve towards each other meeting other cracks at right angles.

Fans. Progressive cracking leading to the development of a fan is illustrated in Figs 4 and 5 for a thin film between a rigid glass slide and a cover slip. The appearance of the fan depends on the angle between the two main edges at which drying occurs. In the example shown in Fig. 5 the edges are at 90° to each other. An example of a fan, formed with the same experimental arrangement, for edges at 65° to each other is shown in Fig. 13. When the angle between the edges is reduced further the fan shape approaches the shape of a chevron. The transition from a fan to a chevron occurs at an angle of about 45° but this is probably an arbitrary effect depending on film thickness and crack spacing.

Inverted fans. As shown in Fig. 2f, an inverted fan is formed when the cracks splay outwards as they grow. The test configuration used to generate this pattern is illustrated in Fig. 14. The cavity, of uniform thickness, was formed between two rigid glass slides. The shape of the cavity was determined by inserting a spacer of polyethylene film. To ensure a good seal between the spacer and the glass the sandwich of glass slides and spacer was clamped together and heated in an oven for 10 min at 150 °C. Melting and flow of the polyethylene occurred. The initial thickness of the film was 60 μm and this reduced to 40 μm during heat treatment. The film was shaped and arranged so that the narrow edge

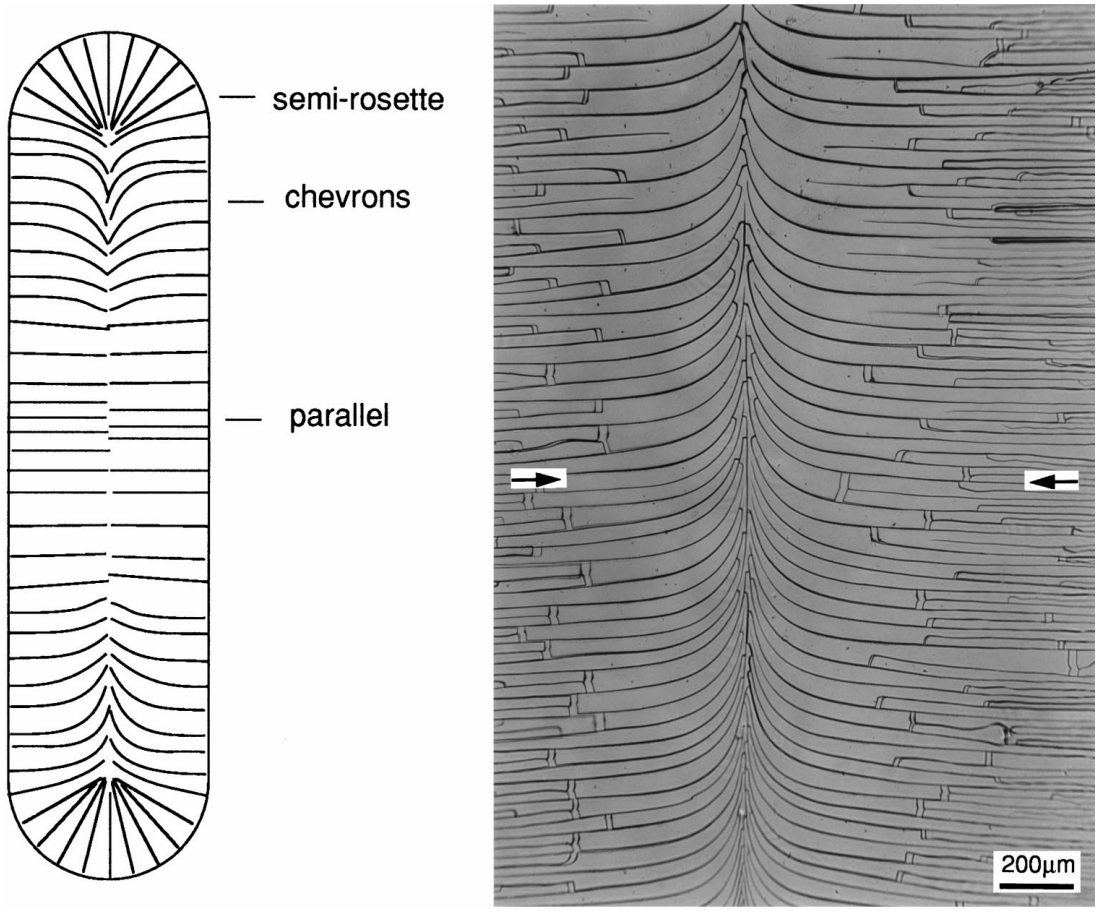

Figure 11 Chevron patterns formed in an uncovered streak: (a) Schematic representation of the arrangement of primary cracks, and; (b) direct observation of crack pattern in a region of chevron cracks.

of the cavity and the bottom of the reservoir were open to the atmosphere. The reservoir region was included to provide extra liquid to feed the shrinkage associated with drying. The cavity was filled with TM-50. The open end of the reservoir was then sealed with adhesive tape. Drying started at the narrow edge (x-y). The cracks developed behind the drying front and spread outwards producing the pattern shown in Fig. 15. The spacing of the cracks is greater than those for the fans shown in Figs 5 and 12 because the thickness of the film is greater.

Two main sets of markings are apparent in Fig. 15: an inverted fan of primary cracks and a set of approximately equal-spaced lines lying normal to the cracks. The second set of markings results from an effect associated with the drying of the sol gel between rigid plates constrained from moving normal to the film by the presence of the polyethylene spacer sheet. The sequence is illustrated in more detail by the example in Fig. 16. Fig. 16a shows the appearance of the 'cracking front' before splaying occurs (cf. Figs 16b and c). The photograph was taken with reflected light and shows sets of fringes in the region ahead of the growing cracks. These result from delamination at one of the sol-gel glass interfaces owing to shrinkage normal to the plane of the film. Delamination occurs in a stop-go mode. At each stop stage additional deformation or damage occurs leaving a fine line. Thus the second set of lines represent successive positions of the delamination front. An early stage of splaying is shown in Fig. 16b and a fully splayed region, viewed in transmitted light is shown in Fig. 16c. Many secondary cracking processes, associated with shrinkage are apparent in Figs 16b and c.

Basins. The experimental arrangement was similar to that used for inverted fans with a cavity shaped as a curved band. Drying occurred from one end of the band which was open to air. Cracks nucleated in this region and grew on curved paths around the basin-shaped region. An example is shown in Fig. 17. Stop-go delamination cracking also occurred as described above and illustrated in Fig. 16a.

5. Discussion

These experiments have produced many observations that require explanation. Detailed analytical descriptions are premature because of the intrinsic complexity of the processes accompanying the development of the cracking patterns and the dearth of information and data on the physical and mechanical properties of drying gels. We are concerned primarily with simulating the patterns of cracks in solidified basalt and in particular with the formation of the primary array of cracks. The problem of secondary cracking that leads to cross-fractures in some basalt columns remains to be resolved. In a two-dimensional analogue the arrays of primary cracks consist of sets of approximately equally spaced lines which may be curved or straight.

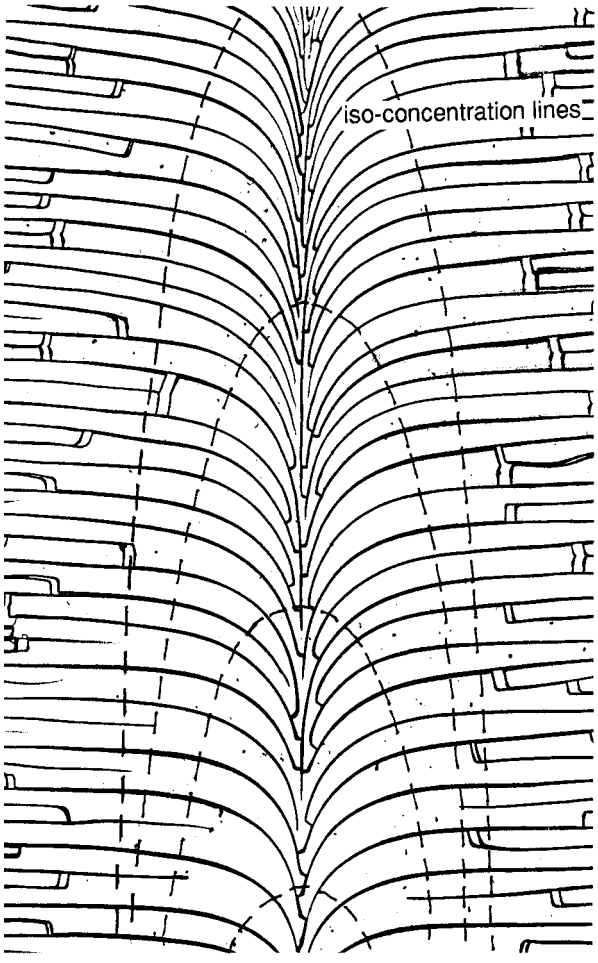

Figure 12 Mapping of the iso-concentration lines on the chevron pattern of primary cracks illustrated in Fig. 11b.

Following Spry [7] and Müller [4] we assume that the shapes of the cracks in the arrays result directly from the shape of the iso-concentration profiles. The pseudo two-dimensional arrays in the sol-gel which simulate the patterns in the basalt, illustrated by Spry, were produced by controlling the drying conditions.

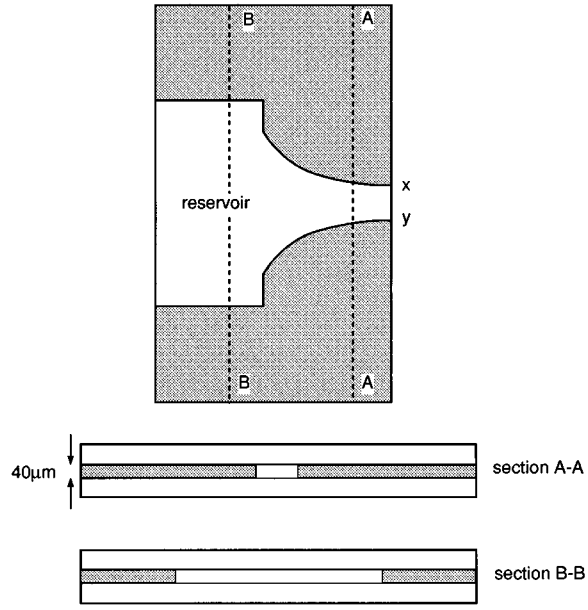

Figure 14 Experimental arrangement used to produce inverted fan patterns.

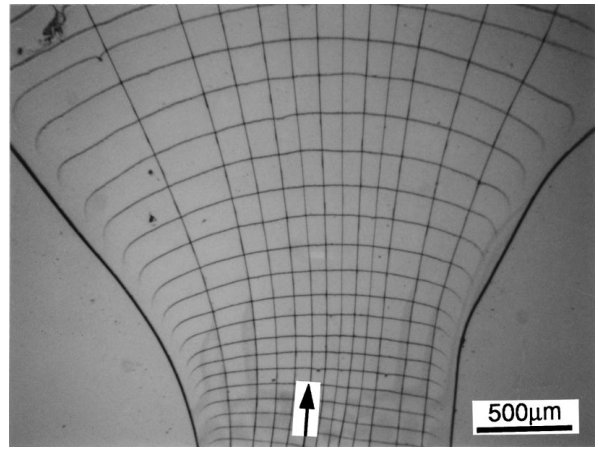

Figure 15 Inverted fan formed in a film of drying sol-gel, of uniform thickness, viewed in transmitted light.

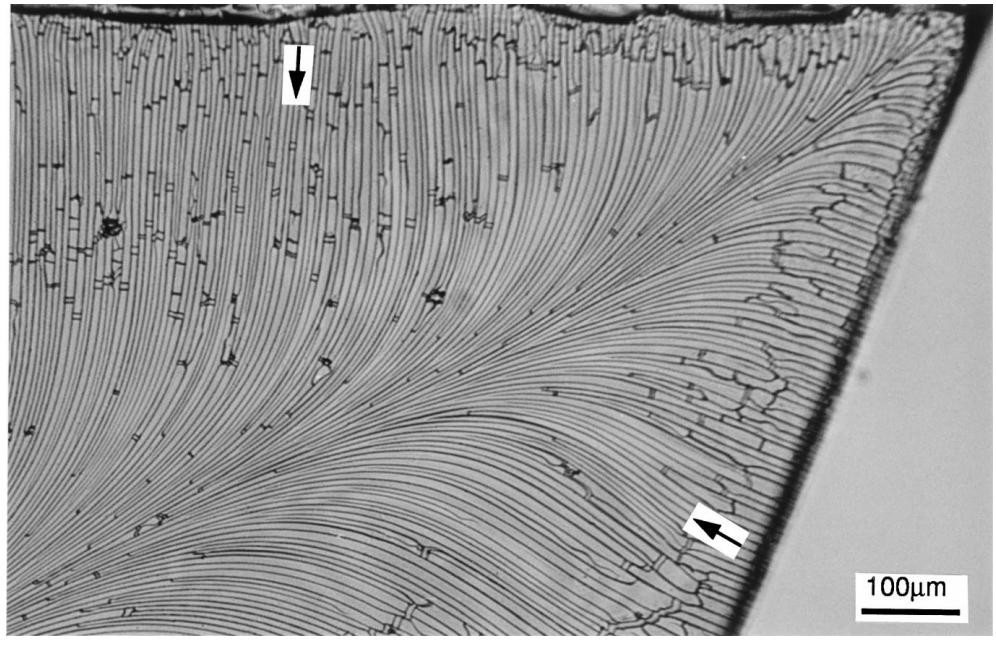

Figure 13 Fan pattern formed between a rigid glass slide and a flexible cover slip with the edges of cover slip cut at 65°.

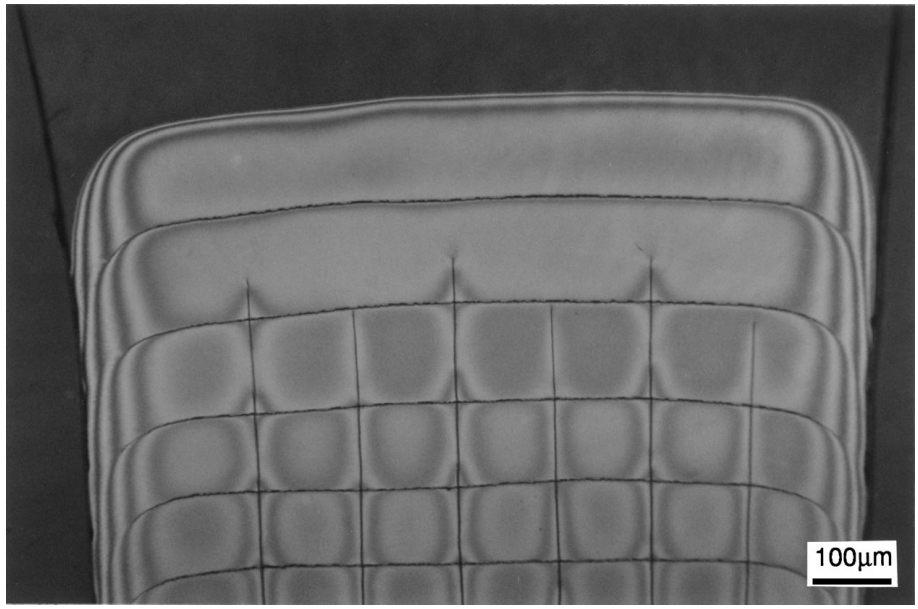

(a)

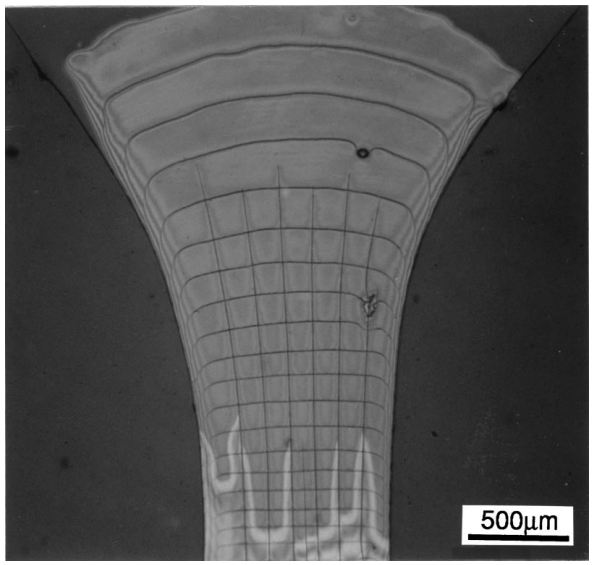

(b)

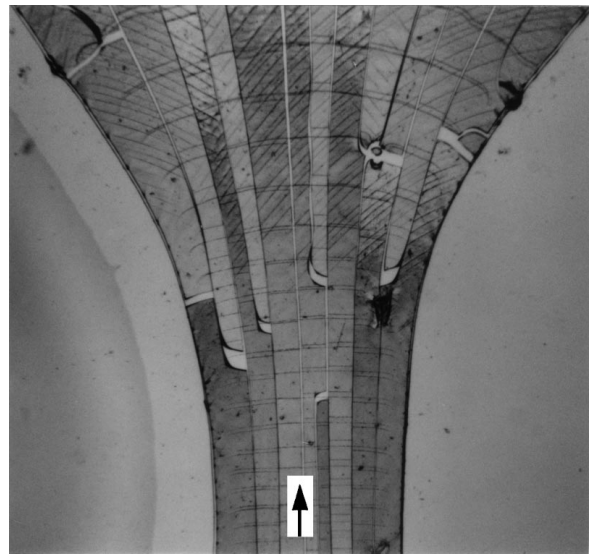

(c)

Figure 16 Progressive development of an inverted fan: (a) Reflected light image of cracking front before splaying has started showing the banded pattern associated with the stop-go progression of delamination cracking; (b) reflected light image of fan formation showing the splaying of the primary cracks, and; (c) transmitted light image of an inverted fan of primary cracks with isolated secondary cracks that formed in the later stages of drying.

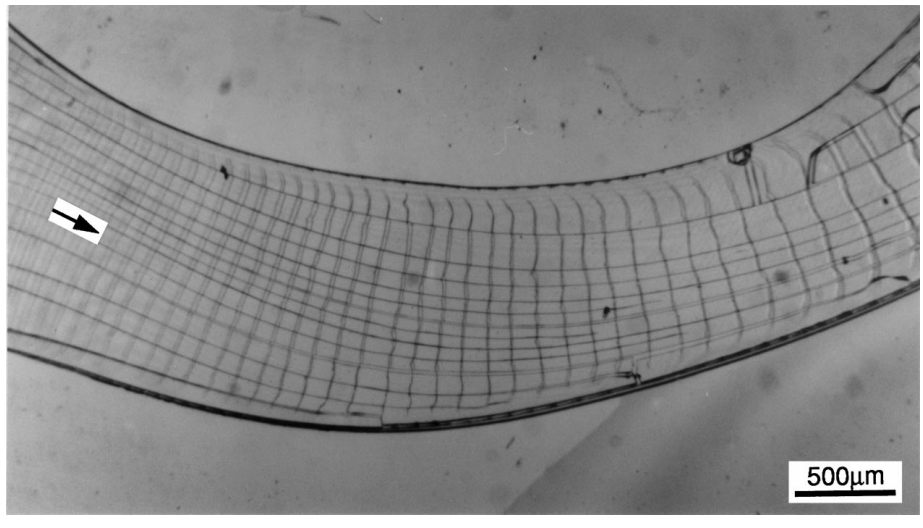

Figure 17 Basin pattern of primary cracks in a film of drying sol-gel, of uniform thickness, viewed in reflected light.

There are three main issues that require further consideration: the origin of the strains that lead to the formation of the primary cracks, the spacing of the cracks and the nucleation of cracks. These effects are best understood in terms of the constraints associated with the geometry of the drying gel and the sequence of cracking processes. In the first stages of drying the liquid shrinks. The liquid flows readily and there are no constraints. In closed cells, such as in the geometry illustrated in Fig. 8a, the volume changes are fully accommodated by liquid flowing to the drying region leaving a cavity at one end of the cell. The viscosity of the liquid increases progressively during desiccation. Eventually the viscosity is so great that volume changes cannot be accommodated by liquid flow. This leads to shrinkage strains that are relaxed initially by plastic or viscoelastic deformation processes. The slip bands (Fig. 9), that form before the onset of cracking, indicate that some of the deformation occurs by plastic flow.

The material exposed to air dries most rapidly and eventually the surface becomes sufficiently rigid that it cannot deform further. Thereafter elastic stresses develop in this layer and, when the strains reach the critical value for fracture, cracks form in the surface layer. Shallow surface cracks in this outer layer grow into less rigid material. The progress of crack growth then depends of the rate of drying and, as illustrated in Fig. 1b, on the drying profiles in the material below the surface.

The elastic strains in the surface layers depend on the geometry of the drying specimen and are critically dependent on the constraints, arising from this geometry, that restrict shrinkage. For the geometry illustrated in Fig. 8a, a drying sol-gel between two rigid plates, the main constraint arises because the gel sticks to the glass surfaces preventing relaxation in the x-direction. Additional constraints are present when the plates are held apart preventing relaxation in the y-direction and also arise-from the layers of partially dried viscoelastic material below the surface, resisting relaxation in the x-y directions. It is the latter constraints that are dominant in controlling the development of cracks in conventional mud cracking. The influence of these additional constraints becomes more important once the primary crack patterns have started to develop.

In the early stages of cracking it is the constraint owing to adhesion to glass that is dominant and is responsible for the formation of an array of approximately equally spaced cracks. The edge of a gel, drying between two rigid plates, is represented by Fig. 18. The dominant shrinkage strain is in the x-direction. This is constrained because the material is bonded to the glass so that stresses develop in the x-direction. As mentioned above additional stresses develop in other directions owing to other shrinkage and Poisson effects. The stresses in the x-direction lead to cracks, parallel to the y-z plane. When the cracks form some of the stresses in the surrounding material are relaxed. Additional stresses develop at the tips of the cracks and these lead eventually to delamination at the gel-glass interfaces.

Before the primary cracks form the stresses in the surface layer are uniform and crack nucleation is random

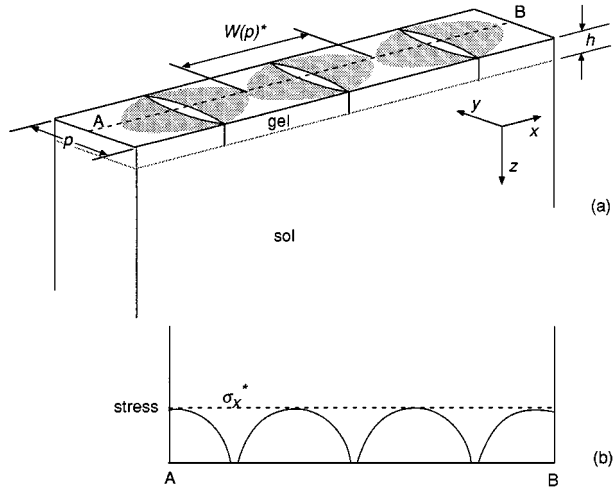

Figure 18 Formation of multiple cracking at edge of a drying sol-gel film between two rigid glass plates: (a) Schematic showing the formation of an array of cracks in the outer crust of dried gel; (b) illustration of stress distribution in the crust when the crack spacing has reached the limiting value.

along the edge of the specimen. Small variations, arising from effects such as microstructural changes, mean that the critical strain for nucleation varies along the edge. Thus, the cracks form sequentially over a small range of shrinkage strains. Stress relaxation around the crack reduces the stresses locally and subsequent cracks do not nucleate in these stress relaxed regions. The distance over which relaxation occurs depends on the strength of the bond between the glass and the gel and the elastic properties of the rigid gel and the glass. This leads to a limiting value of the crack spacing which is related to the shrinkage strain, elastic properties of glass and gel, fracture surface energy and interface strength. The problem is closely related to multiple cracking in composite materials [16] and in the cracking of thin films on substrates [17, 18] but the variations in properties during drying make analysis very complex. Allain and Limat [12] made one such analysis and assumed that the limiting crack spacing was related to secondary drying processes. Observations of the sequence of cracking suggests that this is not a realistic model. According to Allain and Limat's model cracks would form adjacent to each other successively. In practice cracks initiate randomly and progressively fill in until the limiting spacing is reached.

In principle, a value for the limiting spacing can be obtained from an energy balance analysis. Let us assume that the bonding between the glass and the gel is strong enough to prevent interface splitting and that the crack spacing is determined by the cracking of the first formed rigid layer at the surface, depth h (see Fig. 18); presumably cracking occurs at a critical value of h. The strain energy per unit volume resulting from a shrinkage strain of ε_x, neglecting other shrinkage constraints and Poisson effects, is

$$\Psi_s = \frac{1}{2}\varepsilon_x^2 E_x \tag{1}$$

where E_x is Young's modulus of the rigid gel. The energy to form a crack that crosses the thickness of the

film, p, is

$$\Psi_c = hpG_c \tag{2}$$

where G_c is the energy required to form unit area of crack. The elastic strain energy released by the formation of a crack is represented by the shaded area in Fig. 18 which is

$$\Psi_{sw} = W(p)hp\Psi_s = \frac{1}{2}W(p)hp\eta\varepsilon_x^{*2}E_x \tag{3}$$

where $W(p)$ is the length over which relaxation has occurred and η is a shaping factor that depends on the distribution of stress relaxation resulting from the formation of the crack. It is a measure of the efficiency of release of stored energy from the material around the crack. The critical or limiting spacing is determined by equating the total energy of an array of cracks, critical spacing $W(p)^*$, with the elastic energy released by the formation of these cracks. Thus,

$$\psi_c\frac{1}{W(p)^*} = \frac{hpG_c}{W(p)^*} = \frac{1}{2}hp\eta\varepsilon_x^{*2}E_x \tag{4}$$

and

$$W(p)^* = \frac{2G_c}{\eta\varepsilon_x^{*2}E_x} \tag{5}$$

If one assumes a simple linear scaling relationship between $W(p)^*$ and p, and that η is a constant, then $W(p)^*/p$ is a constant and independent of p. The measurements in Fig. 7 suggest that for films between two glass surfaces $W(p)^*/p = 3$. In other geometries $W(p)^*/p$ will have different values because the constraints accompanying cracking are different. One also anticipates that $W(p)^*/p$ will depend on drying conditions, that influence the composition gradients, and on the strength of the bond between the glass and the gel. The diagram in Fig. 18b illustrates the distribution of stress along the centre line of the gel (AB) at the limiting crack spacing. It illustrates that the concept of a limiting crack spacing can be understood in terms of a critical stress σ_x^* for crack nucleation.

The constraints to shrinkage that lead to cracking are strongly dependent on the geometry of the experiment and can change during the drying experiment. Thus, for the geometry discussed above, the orientation of the primary array is associated predominantly with shrinkage in x-direction. Subsequent shrinkage leads to delamination (Fig. 8a) that may occur at both interfaces. This leads to additional desiccation at the delaminated surfaces and a change in the constraints behind the front of growing primary cracks. Various forms of secondary cracking are observed; two modes are illustrated in Figs 8b and c. The development of these additional constraints depends on the flexibility of the glass plates. A variety of secondary patterns result.

Significantly different constraints develop in films of gel on the glass plate without a second rigid glass plate or a cover slip (see Fig. 8d). The rate of desiccation is strongly dependent on the curvature of the surface of the gel and is at a maximum at the sharply curving surfaces at the outer edges of the film. Thus, primary cracking initiates at the edges. In the early stages shrinkage is constrained by the bonding between the film and the glass. Delamination and secondary cracking occurs in the later stages and results in a variety of patterns.

As mentioned previously, the formation of arrays of primary cracks in drying sol-gel were designed to simulate the patterns displayed by basalt formations, as sketched by Spry (Fig. 1). By controlling the test geometry it has been possible to reproduce all of the Spry patterns in the drying gels. The underlying assumption, in designing the experiments, has been that in the arrays of primary cracks the cracks grow normal to the water concentration profiles. This is clearly demonstrated in Fig. 5. The line a-b is one such profile marking the boundary between mobile liquid sol and the relatively immobile partially gelled material. It is intuitively obvious for the other patterns. This conclusion is consistent with the type of explanation offered for basalt column formation as mentioned in the introduction.

Some of the detail in the primary patterns is of interest because of the relation between crack nucleation and the $W(p)^*/p$ effects described above. In the test geometries used to produce the patterns shown in Figs 16 and 17 the film thickness was constant so that one expects the crack spacing to be constant. The initial crack spacing determined from the film thickness is uniform. As the cracks grew into a splayed region (Fig. 16b) it is necessary to nucleate new cracks to maintain the same crack spacing. If nucleation is difficult this process is delayed until further shrinkage constraints are produced (Fig. 16c). In cracking patterns formed with a flexible cover slip (Figs 5 and 13) the thickness of the film varies because the flexible cover slip bends during drying. As the film gets thinner the spacing of the primary cracks decreases. In addition, merging of cracks, as in chevron and fan patterns, means that cracks become more closely spaced as they grow. Some cracks stop growing or curve into another crack and some cracks are nucleated as the primary crack patterns develop to accommodate the requirements for a limiting crack spacing.

6. Conclusions

1. The drying of films of sol-gel can be used to simulate the development of cracking patterns during the solidification of basalt lava flows.

2. By controlling the geometry of the test samples, to create specific drying profiles, it is possible to generate a wide range of primary cracking patterns.

3. The primary cracking patterns, observed in solidified basalt, have been reproduced in sol-gels using a variety of test configurations.

4. The primary and secondary cracking patterns result from the constraints to shrinkage associated with drying. These constraints are related to the drying profiles which are dependent on test geometry. The bonding between the drying sol-gel and the surrounding material strongly influences the development of the constraints.

Acknowledgements

We thank Drs. Bob Murray and Harry Barrow for helpful discussions and Professors Peter Goodhew and David Bacon and their colleagues for allowing us to work in their Department at Liverpool University.

References

1. K. A. GROSSENBACHER and S. M. MCDUFFIE, *J. Volcanology and Geothermal Research* **69** (1995) 95.
2. P. BUDKEWITSCH and P.-Y. ROBIN, *ibid.* **59** (1994) 219.
3. F. W. PRESTON, *J. Soc. Glass. Tech.* **10** (1926) 234.
4. G. MÜLLER, *J. Geophysical Research* **103** (1998) 15239.
5. R. K. ILER, "The Chemistry of Silica" (Wiley, New York, 1977).
6. C. J. BRINKER and G. W. SCHERER, "Sol-Gel Science" (Academic Press, San Diego, 1990).
7. A. SPRY, *J. Geol. Soc. Aust.* **8** (1962) 191.
8. R. MALLET, *Phil. Mag.* **4** (1875) 122 and 201.
9. J. P. IDDINGS, *Amer. J. Sci.* **131** (1886) 321.
10. J. C. JAEGER, *ibid.* **255** (1957) 306.
11. J. D. F. RAMSAY and B. O. BOOTH, *J. Chem. Soc. Faraday Trans.* **79** (1983) 173.
12. C. ALLAIN and L. LIMAT, *Phys. Rev. Letters* **74** (1995) 2981.
13. C. ALLAIN and F. PARISSE, *La Recherche* (1996) pp. 50–52.
14. F. PARISSE and C. ALLAIN, *J. Phys. II France* **6** (1996) 1111.
15. *Idem., Langmuir* **13** (1997) 3598.
16. D. HULL and T. W. CLYNE, "An Introduction to Composite Materials," 2nd ed. (Cambridge University Press, Cambridge, 1996).
17. M. YANAKA, Y. TSUKAHARA, N. NAKASO and N. TAKEDA, *J. Mat. Sci.* **33** (1998) 2119.
18. R. T. MURRAY, C. J. KIELY and M. HOPKINSON, *Phil. Mag.* **74** (1996) 383.

Received 28 January
and accepted 11 May 1999